BJRS

BRAZILIAN JOURNAL
OF
RADIATION SCIENCES
09-03 (2021) 01-18

Experimental apparatus for measurement of photoneutrons from linear accelerator with energy of 16 MeV

Silva[a,b] M.V., Cardoso[b] D.O., Vellozo[b] S.O.

[a]*Universidade Federal do Rio de Janeiro, Av. Horácio de Macedo, 2030, 21941-914, Rio de Janeiro, RJ, Brasil*

[b]*Instituto Militar de Engenharia, Praça Gen. Tibúrcio, 80, 22290-270, Urca-Rio de Janeiro, RJ, Brasil*

E-mail address: *mvilela@coppe.ufrj.br*

ABSTRACT

Particle accelerator technology has a deep impact on society. Its applications are well established mainly in the treatment of cancer and other diseases. This work aims to develop an experimental apparatus with ^{3}He detectors for 16 MeV photoneutron measurements. The apparatus allows us to obtain multienergetic neutrons with the use of a 22 cm diameter spherical attenuator associated with different shield thicknesses. The microscopic processes of the fast and thermal neutrons in the detector were described by the two energy-group diffusion equation. The Detector Response × Dose Rate results show a directly proportional relationship between these two variables with a degree of reliability attested by the linear correlation coefficient $R^2 \geq 0,999$.

Keywords: Particle accelerator, Experimental apparatus, Neutron detectors.

ISSN: 2319-0612
Accepted: 2021-06-25

1. INTRODUCTION

The science of accelerators, as we know, shows profound power of impact on society and this can be seen in the face of their applications that pass both in the midst of science, in general, as well as with regard to the universe of technologies. A good example of this is the significant fraction of radioisotopes manipulated for/in disease treatments, diagnoses and research where so-called accelerators are used. X-ray beams, as well as neutrons, protons and ions derived from particle accelerators, are used for the treatment of cancer and other diseases. In addition, the use of ionizing radiation has been widely used in the medical field, in interventional procedures [1].

Radiotherapy is divided into two modalities: teletherapy and brachytherapy. In brachytherapy, the source of radiation is placed directly in the tumor. The radiation beam is produced by shielded (sealed) radionuclides in order to avoid contamination of the patient with radioactive material [2].

Teletherapy is the use of ionizing radiation, emitted by a device, away from the patient, whose beam is directed to the site to be treated. In this case, ^{60}Co irradiators or linear accelerators are used. It is important to add to this that being the radiation beam attenuated as it penetrates the body, the radiation dose in organs or tissues near the surface is expressive and should be known. For this reason, single beams of radiation are used only in superficial tumors. In deeper tumors a larger number of bundles is recommended for them to be applied in different directions [3]. This being the case, the radiation beams are focused directly on the tumor and the referred dose will be divided there, thus reducing the amount to be destined to healthy tissues, although there is an increase in the total volume of irradiated tissue [4].

In linear accelerators with energies above 10 MeV neutrons occurs due to the interaction of high-energy particles with the various materials of the radiator and the treatment room. These neutrons, here called photoneutrons appear as a contaminant of the treatment beam.

It is known that the production of these neutrons in the particle accelerator does not occur only in the head, but at several points inside [5]. The particles, in the process of interacting with high atomic number materials present in the accelerator, produce, in addition to restraining X-ray photons, neutrons, mainly through the nuclear reaction of the type (γ, n) [6]. Other reactions occur in accelerators that have large amounts of elastic collisions. However, these collisions do not

represent significant energy losses, since they increase the trajectory traveled by neutrons within the shield, producing reactions (n, 2n) [7].

Neutron detection methods are not trivial due to the lack of charges of these particles, as well as the peculiarity of their interactions with matter [8].

The objective of this research was to develop an experimental device designed to correlate the responses of ^{3}He detectors with the measurement of photoneutrons of 16 MeV, as well as the proportionality between them and behavior differences in relation to different moderators of the 3He detector with the measurements of multienergetic neutrons. An analytical model, based on the approximation of the diffusion of two energy groups, was constructed in order to better understand the experimental behavior of the device.

2. MATERIALS AND METHOD

Neutron area monitors are built with three fundamental components: moderator, detector, and the electronic component. The physical principle of area monitor with spherical attenuator is based on the moderation of fast neutrons. To obtain the neutron spectrum it is necessary to perform measurements involving the detector with the various moderator plates. This facilitates detection since detectors are typically much more sensitive to thermal neutrons.

The material responsible for braking neutrons is high density polyethylene and has the function of thermalizing the rapid neutrons through the loss of energy by elastic shocks. Its shape can be spherical or cylindrical, depending on the model of the appliance. There are other types of neutron detectors that use gas enriched with high-section shock materials for thermal neutrons [9].

The materials and equipment used in this work were:

I - Shields composed of five paraffin plates, three paraffin plates and one paraffin plate designated by 5P, 3P and 1P, respectively. Each is 14.5 cm long, 13 cm wide and 3.5 cm thick. Finally, a cadmium plate (1Cd) with 1 mm thickness that serves as shielding (see Figure 3a and 3b);

II - Proportional detection system of type ^{3}He that presents discrimination characteristics (neutrons-gammas). The detector has high efficiency of counts for thermal neutrons and low efficiency for fast neutron counts;

III. Spherical attenuator - Diameter (metric) 22 cm;

IV. Varian linear accelerator, Clinacix model, rated accelerator potential of 16 MeV.

The experimental work was divided into four phases:

a) Assembly of the entire experimental arrangement with paraffin plates (P), Cadmium plate (Cd) and spherical attenuator (E) associated with the detector;

b) Measurement of the thermal neutrons arriving at the fixed detector (^{3}He), depending on the composition of the shielding material, according to the sequence of measurements indicated in tables 1 and 2;

c) Data analysis with the aid of MATLAB programming for the preparation of graphs;

d) Formulation of a model describing the behavior of fast and thermal neutrons in the diffusion approach [10]. This physical process can be verified in Figure 1.

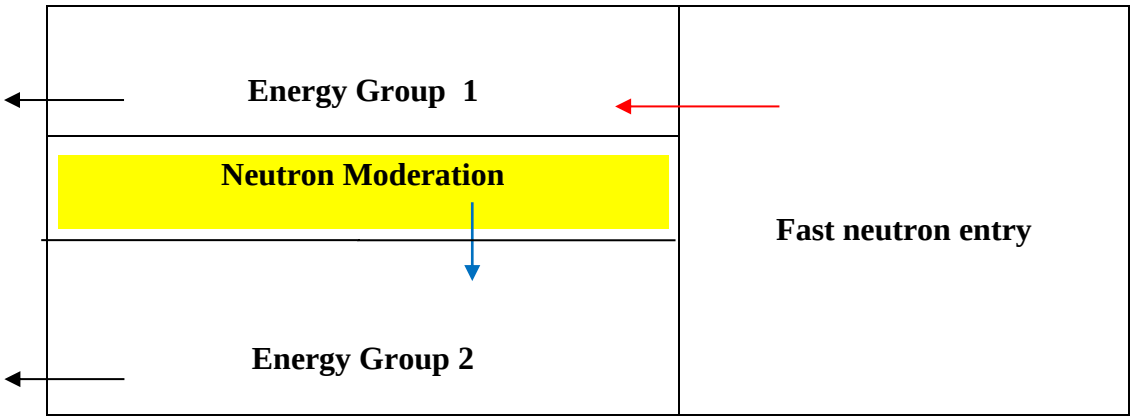

Figure 1*: Illustration of the behavior of fast and thermal neutrons.*

Figure 1 shows, in a squematic way, the entry of neutrons by energy group 1 (fast). Through moderation, group 1 neutrons lose energy and add up to group 2 neutrons, already fully thermalized. The arrows (←) to the left of figure 1 represent the rapid and thermal neutron leaks. This scheme is mathematically described by equations (1) and (2) [10].

$$D_1 \frac{d^2\Phi}{dx^2} + \Sigma_{R1}\Phi = 0 \quad (1)$$

$$D_2 \frac{d^2\chi}{dx^2} + \Sigma_{R2}\chi = \Sigma_{21}\Phi \quad (2)$$

Were,

$\Phi \rightarrow$ Rapid neutron flux;

$\chi \rightarrow$ Thermal neutron flux;

$D_1 \rightarrow$ Diffusion coefficient of energy group 1;

$D_2 \rightarrow$ Diffusion coefficient of energy group 2;

$\Sigma_{R1} \rightarrow$ Macroscopic cross section of energy group removal 1($\Sigma_{R1} = \Sigma_{a1} + \Sigma_{21}$);

$\Sigma_{R2} \rightarrow$ Macroscopic cross section of energy group 2 removal ($\Sigma_{R2} = \Sigma_{a2}$);

$\Sigma_{21} \rightarrow$ Group 1 macroscopic spreading cross section for group 2.

Equations that fix Φ e χ are subject to the following boundary conditions:

$$\Phi(0) = 0, \quad J_1^-|_S = J_1 \quad (3)$$

and,

$$\chi(0) = 0, \quad J_2^-|_S = 0 \quad (4)$$

The reentrant current being S given by:

$$J_1^-|_S = \frac{\Phi}{4} + \frac{D_1}{2}\left(\frac{d\Phi}{dx}\right)_S \quad (5)$$

Equation (5) is the reentrant partial current that represents the source of fast neutrons on the surface S of the design. Analogously, you have the following expression for χ:

$$J_2^-|_S = \frac{\chi}{4} + \frac{D_2}{2}\left(\frac{d\chi}{dx}\right)_S \quad (6)$$

Figure 2 illustrates the physical principle of validation of the experimental apparatus. In the approximation of diffusion to two energy groups, it results in four constants for each region. Contour and media interface conditions (flux and current continuity) allow the system to be determined. The first group must be without the shielding, as it is possible to check the result in Figure 15, and the second group, in turn, considering the complete attenuation system, according to the result shown in figure 16.

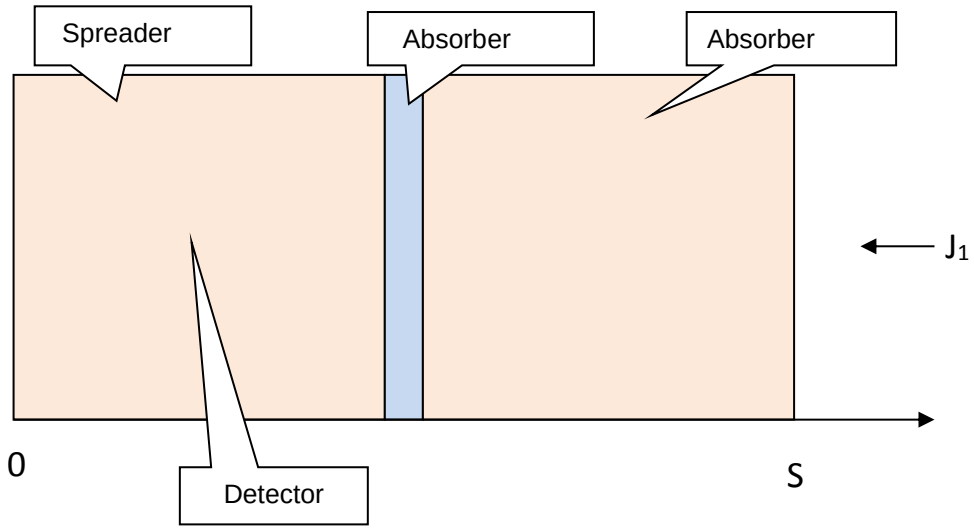

Figures 2: *Model used to represent experimental apparatus* [11].

In the experimental procedure, mobilized here, the energy of 16 MeV was adopted for neutrons of the reentrant partial current J_1^-, in order to measure the leakage current and the beginning of the production of photonêutrons. According to the literature, the production of photoneutrons occurs for photon energies greater than 8 MeV [12]. Then the detector and accelerator reference system, called gantry, initially positioned at angle 0º (see figure 3a). Then the gantry was changed to 270º angle (see figure 3b).

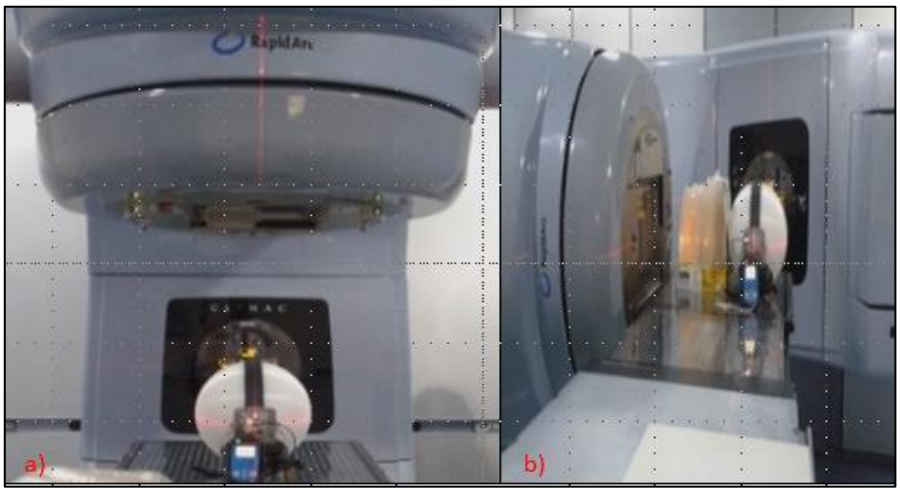

Figures 3: *Illustration of the reference system* [11].

3. RESULTS AND DISCUSSIONS

In this section will be presented the results collected in the activities mentioned in the previous section.

Considering table 1, energy of 16 MeV of the linear accelerator, as well as the fields y = 25.2 cm and x = 5 cm, the results presented in figures 4 to 7 that are below were obtained. Similarly, table 2 shows the fields y = 0.4 cm and x = 5 cm, the results of which are shown in figures 8 -11 and can be observed later.

The correlation index of 0.999 attests to the linearity between the detector response and the efficiency in figures 4 - 11. This experimental response is in full agreement with the predictions of the diffusion model to two energy groups, that is, the increase in the dose rate tends to increase the probability of shock interaction in the head, resulting in the production of photonêutrons.

In addition to linearity, there was an increase in detector count. It is noteworthy that when removing the paraffins plates, there was a decrease in the measurement of thermalized neutrons. This suggests that the neutron flux generated in the head has different energies. The measurements performed directly next to the spherical attenuator indicate that the flux of higher intensity neutrons occurs due to the lower energy photoneutrons produced in the head.

Table 1: Linear Accelerator 16 MeV photon energy (fields y = 25.2 cm and x = 5 cm).

Energy 16 MeV	**Gantry 270º**	**Monitor**	**Gantry 270º**	**Monitor**	**Gantry 270º**	**Monitor**	**Gantry 270º**	**Monitor**
Dose (cGy/min)	**5P+1Cd+E**	**Average**	**3P+1Cd+E**	**Average**	**1P+1Cd+E**	**Average**	**E**	**Average**
100	1919 1922 1904 1927	1918	2006 2022 2015 2008	2012.75	2231 2003 2209 2010	2113	2482 2487 2478 2487	2483.5
200	3800 3780 3798 3788	3791	4027 4031 4024 4030	4028	4572 4518 4531 4445	4516	5065 5077 5083 5058	5070.75
300	6000 5986 5990 5926	5975.50	6472 6080 6054 6090	6174	6875 6881 6803 6824	6845.75	7726 7708 7676 7719	7707.25
400	7950 7931 7941 7997	7959.75	8221 8210 8228 8219	8219.50	9264 9259 9230 9240	9248,25	10400	10400
500	10000	10000	10300	10300	11600 11700	11650	13100 13200	13150
600	12100	12100	12600	12600	14100 14200	14150	16000 16100 16200	16100

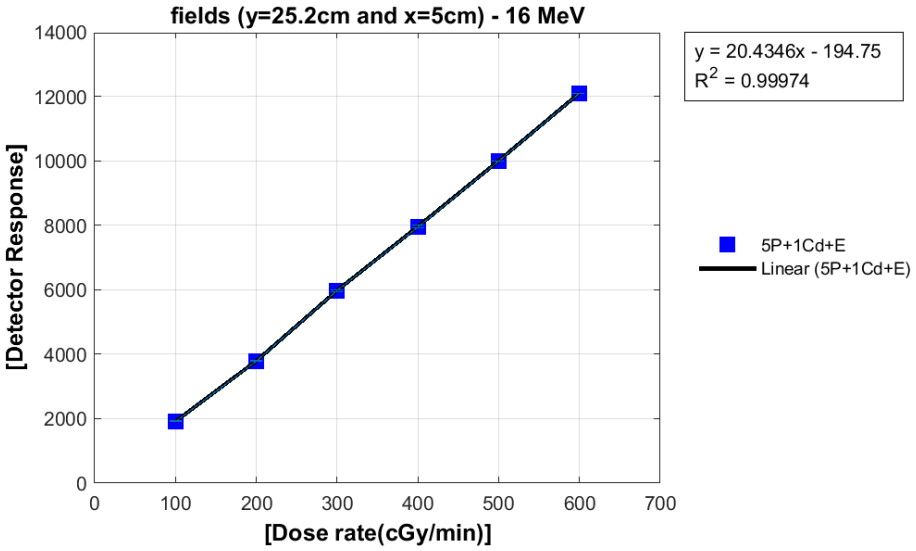

Figure 4: *Shielding with energy beam 16 MeV:5 paraffins, 1 Cadmium, the Sphere.*

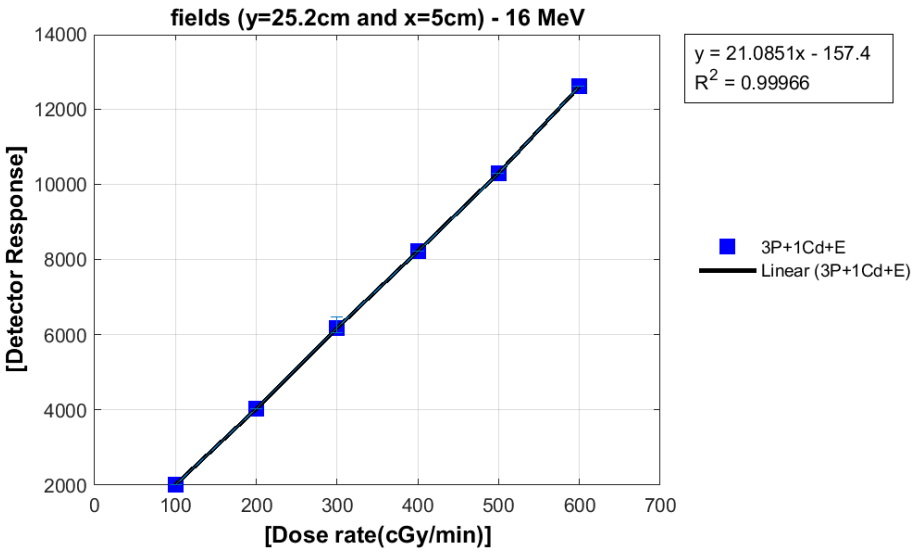

Figure 5: *Shielding with energy beam 16 MeV:3 paraffins, 1 Cadmium, and the Sphere.*

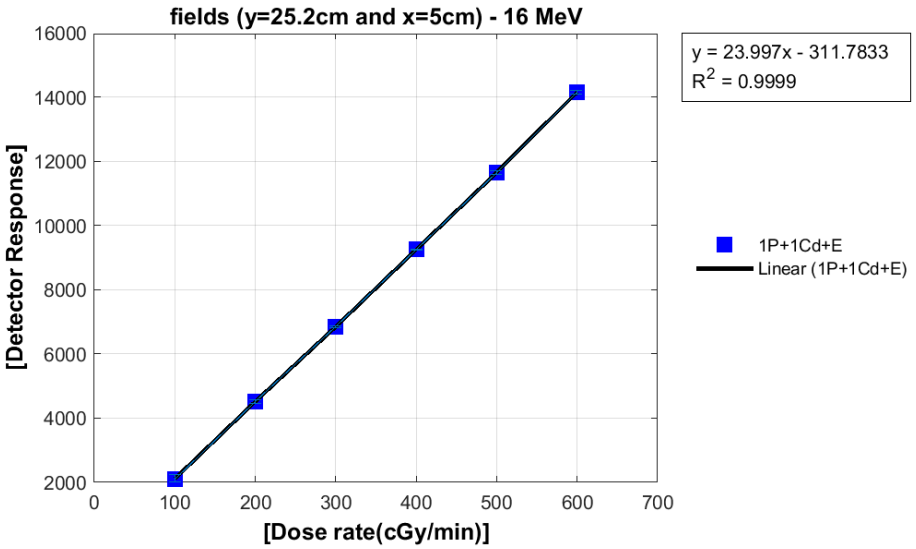

Figure 6: *Shielding with energy beam 16 MeV: 1 paraffin, 1 Cadmium and the Sphere.*

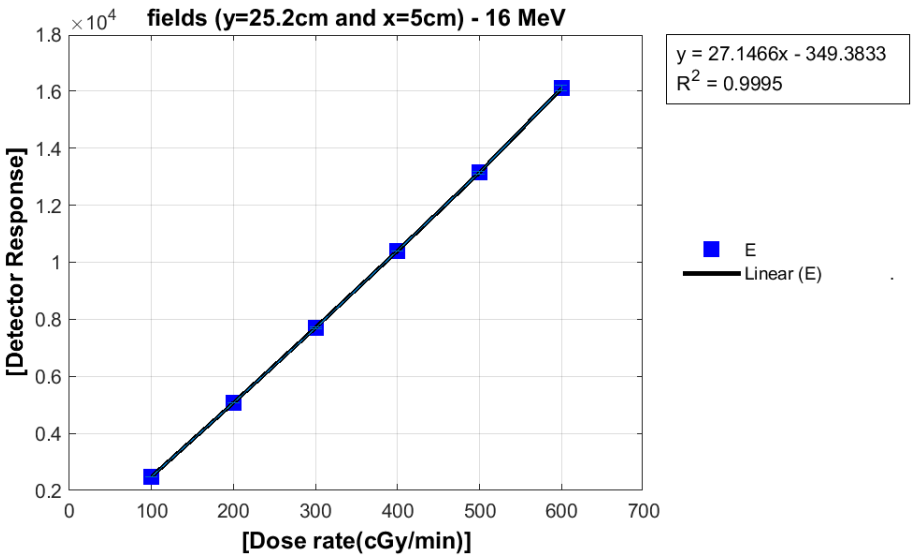

Figure 7: *Shielding with energy beam 16 MeV: Sphere.*

Table 2: Linear accelerator 16 MeV photon energy (fields y = 0.4 cm and x = 5 cm).

Energy 16 MeV	Gantry 270º	Monitor	Gantry 270º	Monitor	Gantry 270º	Monitor	Gantry 270º	Monitor
Dose (cGy/min)	5P+1Cd+E	Average	3P+1Cd+E	Average	1P+1Cd+E	Average	E	Average
100	1911 1908 1917 1916	1913	1944 1950 1941 1936	1942.75	2136 2095 2096 2097	2106	2311 2309 2311 2322	2313.25
200	3791 3809 3836 3788	3806	3914 3859 3850 3953	3894	4274 4223 4012 4081	4147.5	4711 4714 4721 4675	4705.25
300	5776 5741 5730 5736	5745.75	5838 5878 5874 5841	5857.75	6403 6334 6314 6349	6350	7070 7103 7057 7125	7088.75
400	7760 7800 7714 7732	7751.50	7959 7939 7937 7987	7955.50	8492 8529 8536 8536	8523.25	9638 9630 9568 9571	9601.75
500	9800 9814 9809 9851	9818.50	9968 9973 9938 9971	9962.50	10800 10700	10750	12100 12200	12150
600	11900 11800	11850	12000 12100	12050	1100	13100	14600 14800	14700

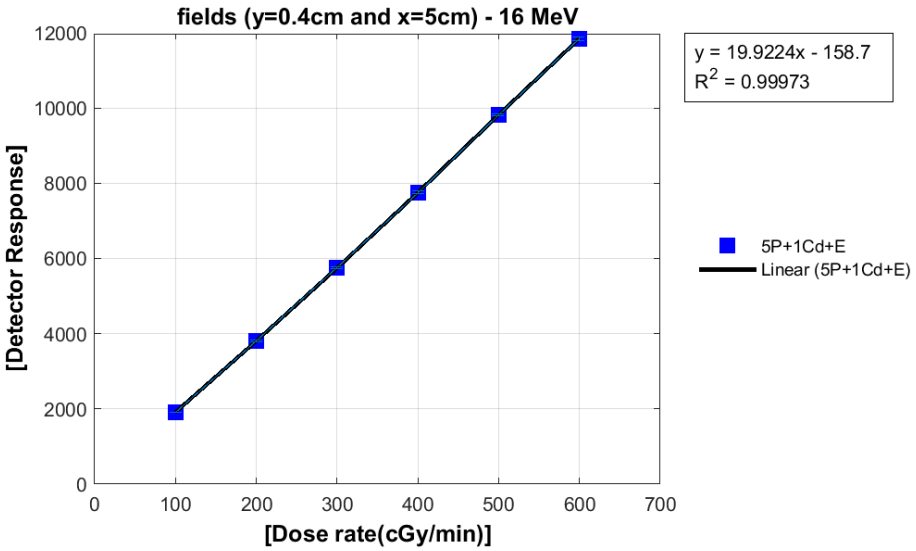

Figure 8: *Shielding with energy beam 16 MeV: 5 paraffins, 1 Cadmium and the Sphere.*

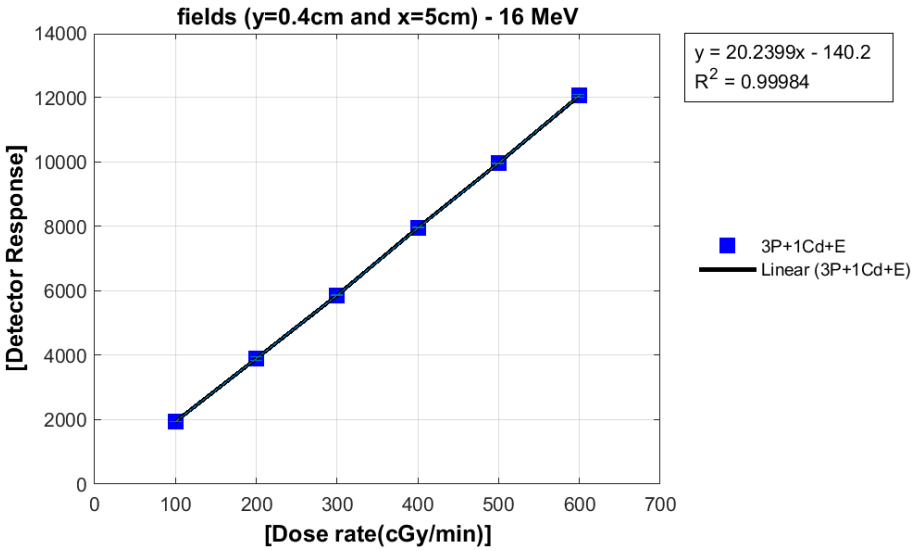

Figure 9: *Energy beam shield16 MeV:3 paraffins, 1 Cadmium, and the Sphere.*

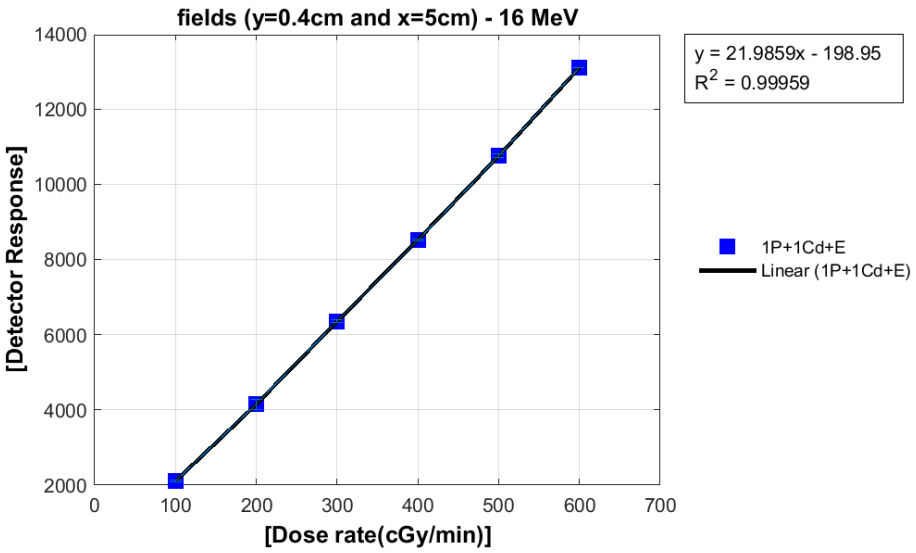

Figure 10: *Energy beam shield16 MeV:1 paraffin, 1 Cadmium, and the Sphere.*

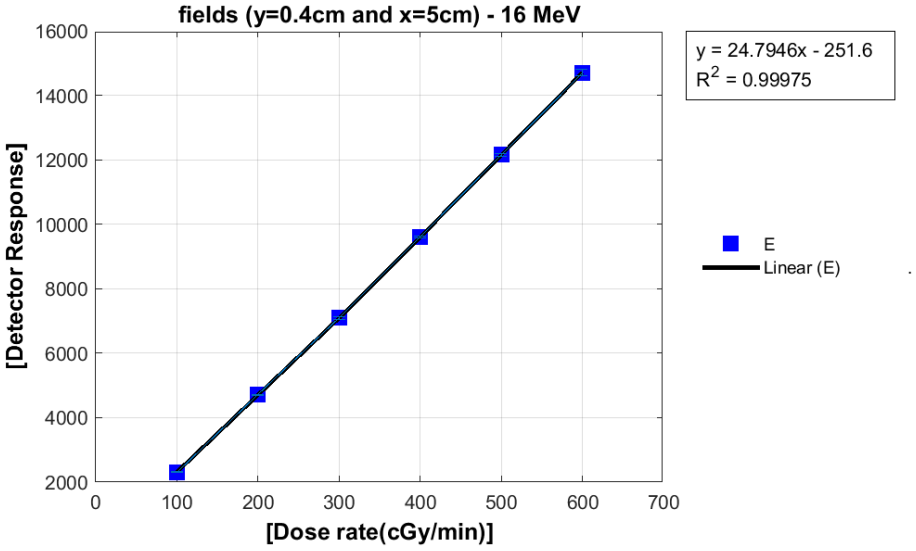

Figure 11: *Shielding with energy beam 16 MeV: Sphere.*

As can be seen, the correlation coefficient showed to be 0.999 in figures ranging from 4 to 11, with variations only in the fourth decimal place. This proves the related relationship between x and y, within the required precisions. Figures 12 and 13 show a growth behavior in the response due to the different neutron attenuations for different dose rates.

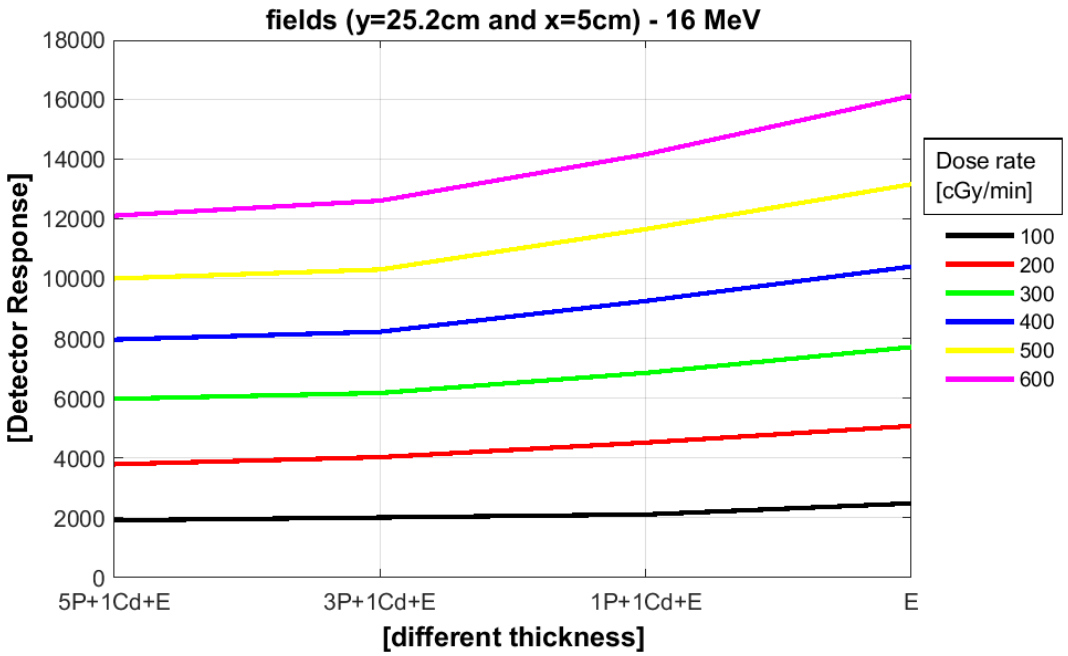

Figure 12: *Different dose rates with different neutron attenuator thicknesses.*

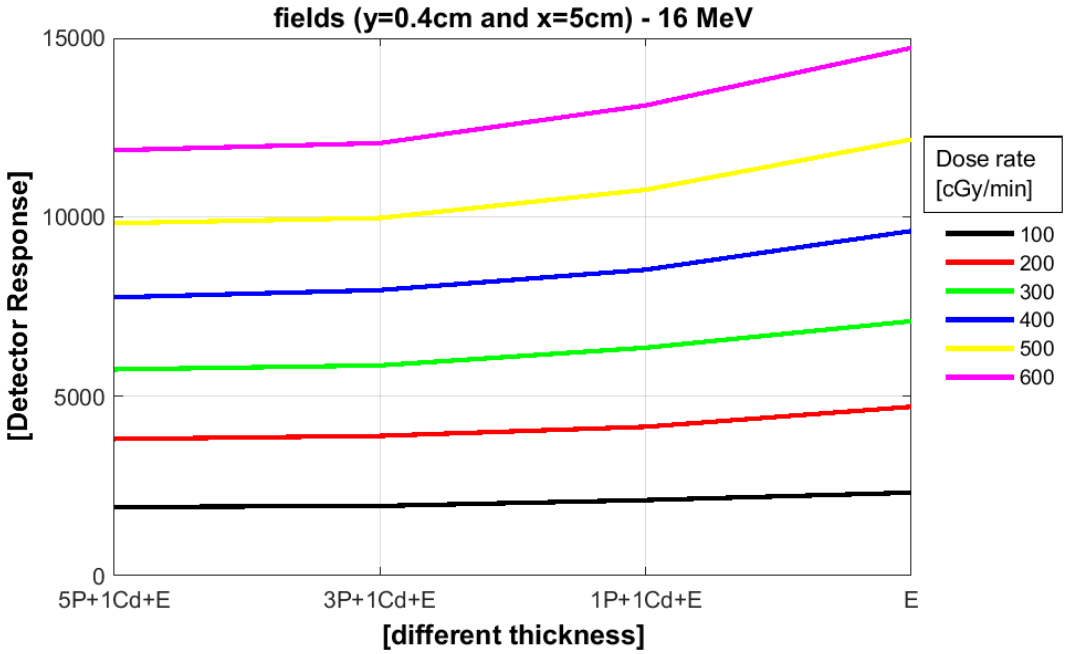

Figure 13: *Different dose rates with different neutron attenuator thicknesses.*

Figure 14 presents different detector responses for different dose rates and different neutron attenuator thicknesses. It is noteworthy that the standard behavior of radiation attenuation, in this case, neutrons, follows the exponential law.

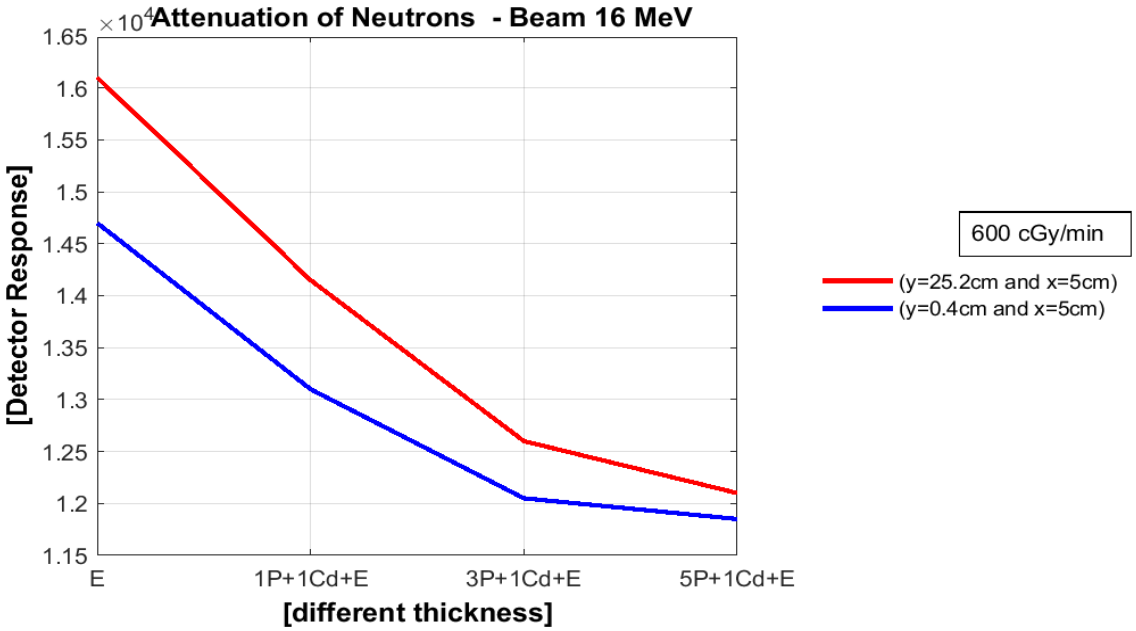

Figure 14: *Shields with different fields.*

In order to validate the methodology under discussion, the experimental results were compared with the theoretical model in the approximation of diffusion. A figura 15 mostra o que acontece com os fluxos Φ e χ na ausência de placas de parafina, ou seja, pouca termalização dos nêutrons. Em contraste, a figura 16 mostra um cenário bem diferente quando se adicionam as placas de parafina. Grande parte dos nêutrons são termalizados aumentando, consideravelmente, o fluxo térmico χ. Apesar de qualitativo o modelo explica, de forma simples, a razão das variações de χ.

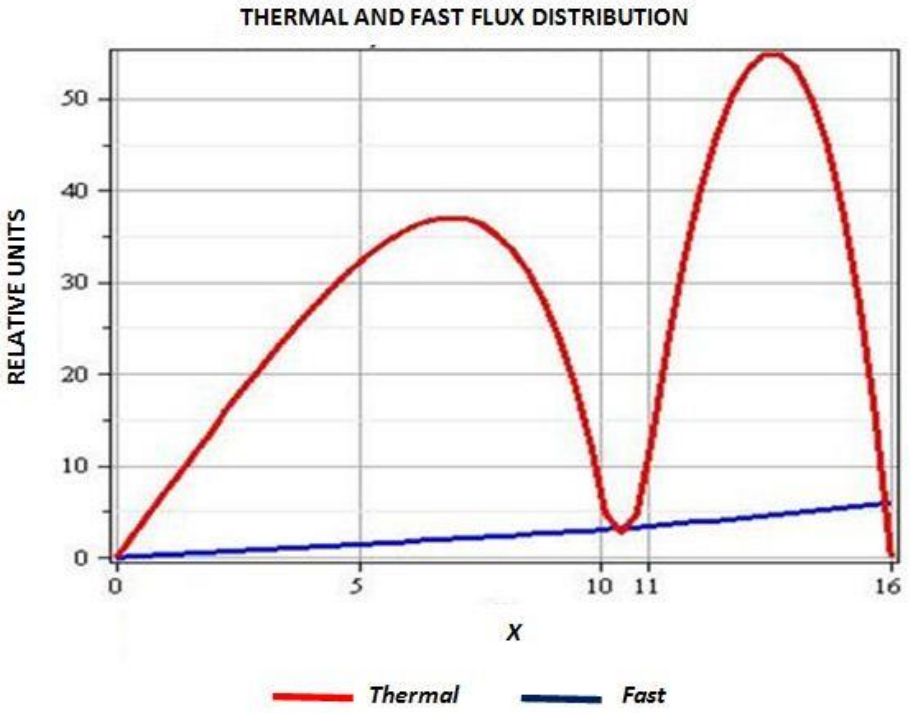

Figure 15: *Graphs of the rapid and thermal flux distribution without the thicknesses of paraffins.*

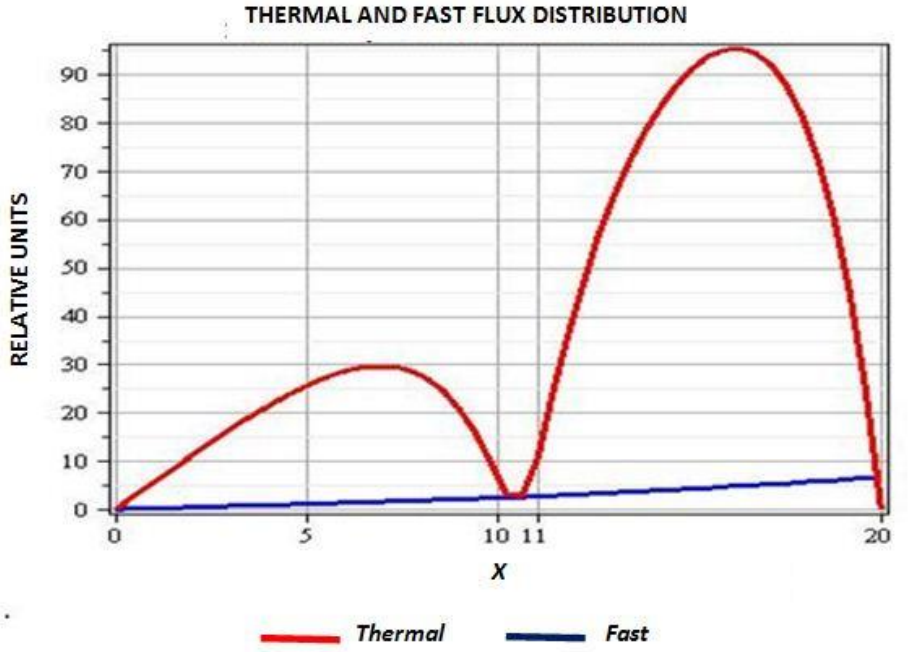

Figure 16: *Graphs of the rapid and thermal flux distribution with the complete thicknesses of paraffins.*

4. CONCLUSIONS

A single series of measurements was performed on the linear accelerator. This machine only offers the rated potential of 16 MeV. The results showed a proportional correlation between the detector response caused by photoneutrons and the dose rate with correlation coefficient $R^2 \geq 0{,}999$. In addition, the results show that the influence of photon measurement on the neutron detector (gamma radiation) should be better investigated.

A proposal to evaluate the influence of gamma radiation would be:

1- Redo the measurements with the accelerator at 16 MeV energy, threshold energy for photogeneration of photons whose same photon intensity of 16 MeV was used in this work;

2- Irradiate the equipment to evaluate the gamma field, in order to verify the discrimination of the neutron detector.

This experimental apparatus allowed the obtaining of a multi-energy neutron measurement procedure using the same detector and changing the different thicknesses (attenuators) of paraffin shielding for different rates of radiation doses. It was also observed that the tungsten collimators used in the accelerator did not serve as shielding for neutrons. Due to this presence of neutrons, healthy organs are also irradiated, and may generate some kind of damage in the patient undergoing treatment. This fact evidenced in Thalhofer's dissertation [13]. We also understand that this finding points to a right in the proposal of the methodology under development.

REFERENCES

[1] UNSCEAR - United Nations Scientific Committee on the Effects of Atomic Radiation Sources and effects of ionizing radiation. **Report to the General Assembly, with scientific annexes.** Volume I: Report to the General Assembly, Scientific Annexes A and B. 2008.

[2] MORTON, G.C., et al., **Health-related quality of life after single-fraction high-dose-rate brachytherapy and hypofractionated external beam radiotherapy for prostate cancer.** International Journal of Radiation Oncology Biology Physics, 2011.80(5): p. 1299-1305.

[3] PERES, L., **Ionizing radiation: physical principles, applications and risks.**1a ed. Celd. 2008.

[4] ZHANG, X., et al., **A methodology for automatic intensity-modulated radiation treatment planning for lung cancer. Physics in Medicine and Biology,** 2011.56(13): p. 3873-3893.

[5] REBELLO, W. F**., Shielding for the protection of neutron patients generated from linear accelerators used in radiotherapy.** 2008. 78 p. Thesis (Doctorate in Sciences) - Federal University of Rio de Janeiro, Graduate Program of Nuclear Engineering, COPPE, 2008.

[6] National Council on Radiation Protection and Measurements. **Neutron contamination from medical accelerators.** Bethesda, MD: NCRP Report. no. 79; 1984.

[7] FACURE, A.N.S.S., **Occupational doses due to neutrons in linear accelerator rooms for medical use.** 2006. 125 p. Thesis (Doctorate in Sciences) - Federal University of Rio de Janeiro, Graduate Program of Nuclear Engineering, COPPE, 2006.

[8] ZAMBONI, C.B., 2007, **Fundamentals of Neutron Physics,** 1 ed., São Paulo, Editora Livraria da Física.

[9] SALGADO, A. P**., Evaluation of the response of area monitors to neutrons in radiation field generated by a clinical accelerator of 15 MV.** 2011. 58 p. Dissertation (Master)- Institute of Radioprotection and Dosimetry, 2011.

[10] DUDERSTADT, J. J., HAMILTON, L.J., Nuclear Reactor Analysis. Wiley, 1976.

[11] SILVA. M.V., **Proposal of experimental device for characterization of the response of 3He detectors, for measurement of photoneutrons generated in accelerators with energy above 8 MV.** 2016. 77 P. Thesis (Nuclear Master) - Military Institute of Engineering, Rio de Janeiro, 2016.

[12] ICRU. ICRU Report 83: **Prescribing Recording and Reporting Photon-Beam Intensity-Modulated Radiation Therapy (IMRT).** Oxford University Press. Journal of the ICRU. 2010;10(1):17-38.

[13] THALHOFER, J.L., **Calculation of Doses in Healthy Organs in Radiotherapy Treatment for Prostate, Using Computational Modeling and Fantoma in Voxel.** 2011. 83 p. Thesis (Master of Science) - Military Institute of Engineering, Section of Nuclear Engineering, 2011.